Instabilities of Stationary Inviscid Compressible Flow around an Airfoil

R. van Buuren, J. G. M. Kuerten, and B. J. Geurts

Faculty of Applied Mathematics, University of Twente, P.O. Box 217, Enschede, 7500 AE, The Netherlands
E-mail: r.vanbuuren@math.utwente.nl

In this paper we numerically solve the stationary inviscid flow around an airfoil. Using the second-order explicit Runge–Kutta method in combination with the MUSCL scheme and the minmod limiter, we do not obtain a machine accurate solution. This has already been observed in literature and is explained by the non-differentiability of the minmod limiter. An analysis of the limiter shows that it is possible to obtain a machine accurate solution with an asymmetric minmod limiter if an implicit scheme with low CFL number is used. For higher CFL number the convergence rate of this scheme increases considerably at the expense of a strong increase in the final residual level. A further study of the differences reveals that the steady state obtained with the implicit method is in fact unstable and can only be found due to the dissipation present in the implicit method. In this paper we give some evidence that the stall in convergence with the explicit method might be caused by a physical instability in the wake behind the airfoil. This instability is also predicted by linear stability theory and confirmed by a grid refinement study.   © 1997 Academic Press

Key Words: Physical instabilities; inviscid flow; TVD schemes.

1. INTRODUCTION

In the previous two decades computation time required to calculate the steady-state solution to the Euler and Navier–Stokes equations has decreased enormously, not only due to more powerful computers but also through the use of, e.g., multigrid, implicit methods or combinations of these two. Moreover, highly accurate schemes have been developed in order to capture shocks in transonic flow applications. The introduction of higher order TVD schemes for transonic flow applications

520

enables the combination of two desirable features of a numerical scheme: a minimal amount of artificial dissipation and monotonicity preservation which eliminates numerical oscillations near shocks. Examples of such TVD schemes which are commonly used are ENO schemes [17] and MUSCL schemes [2]. Both types of schemes incorporate a non-linear function which limits gradient differences of the solution between adjacent cells. It can be shown that the graph of this limiter should satisfy specific constraints in order to be of higher order and monotonicity preserving. This still leaves a certain freedom in the choice of the limiter. Commonly used limiters in literature are the superbee of Roe, Van Albada's limiter, the minmod limiter, and Van Leer's limiter [18]. These limiters can be divided into two groups, differentiable or non-differentiable limiters.

In spite of these favourable properties of TVD schemes, it is often remarked in literature that the limiter may inhibit convergence to steady state. In references [3, 4] it is remarked that a non-differentiable limiter inhibits convergence to steady state independently of the time integration. To obtain a steady-state solution references [3, 4] use a differentiable limiter. Conversely, employing a multi-grid technique and an optimized explicit time integration scheme Park and Kwon [16] obtain a steady-state solution for a large class of limiters, including non-differentiable limiters. In this paper we show that with a proper implicit scheme it is also possible to obtain a machine accurate steady-state solution for the Euler equations with the non-differentiable minmod limiter.

Eriksson and Rizzi [15] have developed an approximate eigenvalue analysis for a semi-discrete centered finite volume scheme and adopted this to transonic inviscid flow around an airfoil. They observed that there are modes which are not damped well and correspondingly dominate the asymptotic convergence to steady state. These modes appeared to be centered around the shock, the wake, and the stagnation point of the airfoil and have eigenvalues with a very small negative real part. They conclude that the addition of aritificial dissipation or the application of local time stepping is beneficial for convergence because it decreases the real part of the eigenvalues of these modes, thus damping them better.

We show, conversely, that methods which do obtain a machine accurate steady-state solution in fact may add too much artificial dissipation. By studying the differences in the solution obtained with an explicit Runge–Kutta time stepping scheme and an implicit method there appears to be a weak instability in a region behind the trailing edge. On a coarse grid with a resolution comparable to the finest grid in [15] instabilities show up near the shock and stagnation point but these regions of instabilities disappear when refining the grid. A grid refinement study shows that the region of instability does not vanish on a very fine grid. These instabilities are also confirmed by linear stability theory (LST).

The contents of this paper are as follows. In Section 2 we state the governing equations and the numerical method for the explicit Runge–Kutta scheme. In Section 3 numerical results for the explicit scheme are presented and the convergence level of the residual will be compared with results obtained with other numerical methods in literature. In Section 4 an implicit scheme is introduced with which a machine accurate solution with the non-differentiable minmod limiter can be obtained. Section 5 contains a discussion of the numerical results for the implicit

scheme and a comparison study of the final residual levels obtained by the implicit and explicit methods. Finally, in Section 6 the conclusions are summarized.

2. GOVERNING EQUATIONS AND EXPLICIT NUMERICAL METHOD

In this section we state the equations governing inviscid compressible flow and specify the time explicit numerical method. Although we are interested in the stationary solution for the flow around an airfoil we do not solve the stationary equations directly. Instead, we start from an initial condition and use a time stepping scheme to obtain the stationary solution.

Governing Equations

The equations governing inviscid compressible flow are the Euler equations. In Cartesian coordinates in two dimensions they read,

$$\frac{\partial q}{\partial t} + \frac{\partial f}{\partial x} + \frac{\partial g}{\partial y} = 0 \tag{1}$$

with

$$q = \begin{bmatrix} \rho \\ \rho u \\ \rho v \\ E \end{bmatrix}, \qquad f = \begin{bmatrix} \rho u \\ \rho u^2 + p \\ \rho u v \\ u(E + p) \end{bmatrix}, \qquad g = \begin{bmatrix} \rho v \\ \rho u v \\ \rho v^2 + p \\ v(E + p) \end{bmatrix}, \tag{2}$$

where ρ is the density, E is the total energy density, and u and v are the velocity components in the x and y direction, respectively. The constitutive equation for the pressure, p, is given by

$$p = (\gamma - 1) \left(E - \frac{1}{2} \rho(u^2 + v^2) \right), \tag{3}$$

where γ is the adiabatic gas constant, which we take $\gamma = 1.4$.

Spatial Discretization

The Euler equations in (1) are in conservation form where the state vector q contains the densities of the conserved quantities and f and g are the corresponding flux vectors. Integration of (1) over an arbitrary volume in space shows that the components of q change only due to a flux through the boundaries of this volume.
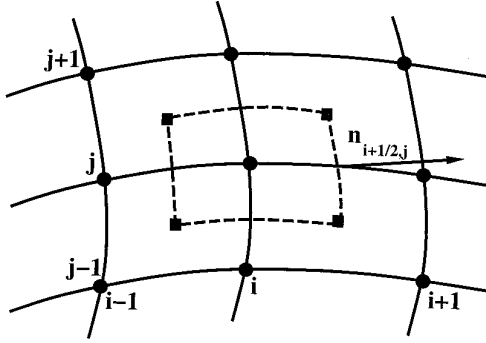
FIG. 1. Control volume for grid point (i, j). The arrows denote the normals on the edges.

To solve (1) we use a finite volume method on a structured grid that computes the flux over the control volume edges as in Fig. 1,

$$\Omega_{i,j} \frac{dq_{i,j}}{dt} + h_{i+1/2,j} - h_{i-1/2,j} + h_{i,j+1/2} - h_{i,j-1/2} = 0, \tag{4}$$

where $\Omega_{i,j}$ is the volume of the control volume and h is the numerical flux vector on the four boundaries segments $(i + \frac{1}{2}, j)$, etc.

In transonic flow applications shocks may occur. These shocks demand certain features of the numerical scheme. First, the shock must be properly located. Second, the scheme has to suppress numerical oscillations near the shock. By construction, scheme (4) is automatically in conservation form. This is a necessary condition for a proper capturing of the shock [5]. To suppress numerical oscillations near the shock, artificial dissipation can be added explicitly or implicitly by the use of upwind schemes. First-order upwind schemes suppress these oscillations but smear the shock. This can be avoided if a higher order TVD (Total Variation Diminishing) scheme as, e.g., developed by Van Leer [2] is used. This type of higher order scheme uses a non-linear function which limits gradient differences of the solution between adjacent cells. The class of limiters can roughly be divided into two groups [5]: differentiable limiters, e.g., Van Leer's limiter, or non-differentiable limiters, e.g., the minmod limiter which we use in this paper.

The numerical flux on the control volume edges is approximated using the flux splitting method of Roe [6], e.g.,

$$h_{i+1/2,j} = \frac{1}{2} l_{i+1/2,j} \begin{bmatrix} f(q_l) + f(q_r) \\ g(q_l) + g(q_r) \end{bmatrix} \cdot \mathbf{n}_{i+1/2,j} - \frac{1}{2} l_{i+1/2,j} |A_{i+1/2,j}|(q_r - q_l), \tag{5}$$

where $l_{i+1/2,j}$ is the length of the control volumes edge, $\mathbf{n}_{i+1/2,j}$ is the normal on the edge, q_l and q_r are appropriate left and right state vectors, the dot denotes the inner product, and $A_{i+1/2,j}$ is the combined flux Jacobian obtained by taking the Jacobian of the inner product of the normal with the flux vector on the control volume edge. The absolute value of the flux Jacobian matrix is defined as $|A| = $

$R|\Lambda|L$, where R and L are right and left eigenvector matrices of A and $|\Lambda|$ is a diagonal matrix containing the absolute values of the eigenvalues of A. As a result of this projection the flux Jacobian becomes a function of q_l, q_r, and the normal $\mathbf{n}_{i+1/2,j}$

$$A_{i+1/2,j} = A(q_l, q_r, \mathbf{n}_{i+1/2,j}) = A(q_{lr}, \mathbf{n}_{i+1/2,j}), \tag{6}$$

where $q_{lr} = q_{i+1/2,j}$ denotes Roe's average state vector which is determined by calculating the primitive variables according to

$$u_{lr} = \frac{u_l + du_r}{1 + d},$$

$$v_{lr} = \frac{v_l + dv_r}{1 + d}, \tag{7}$$

$$H_{lr} = \frac{H_l + dH_r}{1 + d}$$

with $d = \sqrt{\rho_l/\rho_r}$ and H the specific enthalpy. For the first-order approximation of the flux the left state vector q_l equals $q_{i,j}$ and the right state vector q_r equals $q_{i+1,j}$. To achieve a higher order monotonic upwind method we interpolate the state vector with the MUSCL scheme [2] using the minmod limiter

$$q_l = q_{i,j} + \frac{1}{4}[(1 - \eta)\,\text{Lim}(\Delta q_{i-1/2}, \omega\,\Delta q_{i+1/2}) + (1 + \eta)\,\text{Lim}(\Delta q_{i+1/2}, \omega\,\Delta q_{i-1/2})], \tag{8}$$

$$q_r = q_{i+1,j} - \frac{1}{4}[(1 - \eta)\,\text{Lim}(\Delta q_{i+3/2}, \omega\,\Delta q_{i+1/2}) + (1 + \eta)\,\text{Lim}(\Delta q_{i+1/2}, \omega\,\Delta q_{i+\frac{3}{2}})] \tag{9}$$

with $\Delta q_{i+1/2,j} = (q_{i+1,j} - q_{i,j})$ and the limiter is defined as

$$\text{Lim}(a, b) = \frac{1}{2}(\text{sign}(a) + \text{sign}(b))\min(|a|, |b|). \tag{10}$$

The parameters η and ω must obey

$$-1 \leq \eta \leq 1,$$

$$1 \leq \omega \leq \frac{3 - \eta}{1 - \eta} \tag{11}$$

to ensure monotonicity [14]. For the special choice of $\eta = \frac{1}{3}$ the scheme is third-order accurate in smooth regions. In this paper we will use: $\eta = \frac{1}{3}$ and $\omega = \frac{3}{2}$, unless stated otherwise.

If we apply Roe's scheme (5) to the convective part, $a(\partial u/\partial x)$, of the one-dimensional advection equation with $a > 0$, we get $a(u_{l,i+1/2} - u_{l,i-1/2})$. Substitution of (8) gives for this term
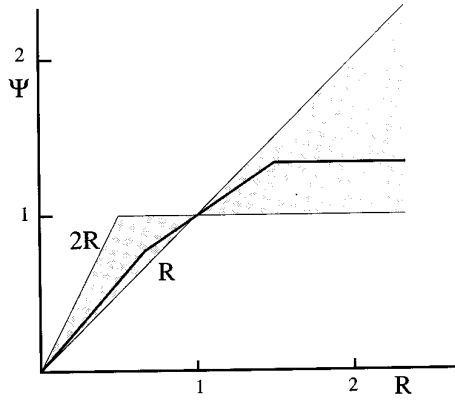
FIG. 2. Region for the limiter in order to obtain a second-order TVD (shaded) method and the asymmetric minmod limiter with parameters $\omega = \frac{3}{2}$ and $\eta = \frac{1}{3}$ (solid line).

$$\frac{a}{\Delta x} \left[1 + \frac{1}{2} \psi(R_i) - \frac{1}{2} \frac{\psi(R_{i-1})}{R_{i-1}} \right] (u_i - u_{i-1}) \tag{12}$$

with Δx the grid size,

$$\psi(R_i) = \frac{1}{2} [(1 - \eta) \, \mathrm{Lim}(1, \omega R_i) + (1 + \eta) \, \mathrm{Lim}(R_i, \omega)], \tag{13}$$

and $R_i = (u_{i+1} - u_i)/(u_i - u_{i-1})$. Clearly, since $a > 0$, the term between brackets in (12) must be positive in order for the scheme to be TVD. This results in the constraint

$$0 \le \psi(R) \le 2R \tag{14}$$

which gives the upper bound for ω in (11). Second-order accuracy in space is obtained if $\psi(1) = 1$. It is easily verified that the limiter (13) satisfies this condition for all η and ω obeying (11). Moreover, Sweby [18] shows that the limiter, ψ, must lie between 1 and R. Together with the previous constraint (14) this yields the shaded region in Fig. 2. This is the well-known second-order TVD region [5] in which the limiter must lie. A time stepping scheme may result in an additional constraint on the limiter. In references [5, 18] the time stepping method results in an upper bound of $\psi \le 2$ arising from stability requirements. For an implicit scheme such as Euler backward there is no upper bound on the limiter, which is in agreement with the A-stability of this scheme.

For a smooth part of the steady-state solution, where smooth is defined as slowly varying on the scale of the mesh size, the quotient R is close to one. The lower bound of the TVD region in Fig. 2 is the original minmod limiter, which corresponds to the choice $\omega = 1$ for all η. The original minmod limiter is non-differentiable only for $R = 1$. If we choose $\omega \ne 1$ the limiter (13) becomes asymmetric. We have plotted the graph of the limiter for the specific choice of $\omega = \frac{3}{2}$ and $\eta = \frac{1}{3}$. It shows

that the limiter is still non-differentiable but it is a smooth linear function in a neighborhood of $R = 1$.

Time Integration

For the time integration we use a second-order accurate explicit four stage compact storage Runge–Kutta scheme. The time step of the explicit scheme is bounded for stability reasons and for the control volume $\Omega_{i,j}$ it is chosen such that

$$\Delta t_{i,j} = \frac{\sigma \Omega_{i,j}}{\max(l_{i+1/2,j}\lambda_{i+1/2,j}, l_{i-1/2,j}\lambda_{i-1/2,j}) + \max(l_{i,j+1/2}\lambda_{i,j+1/2}, l_{i,j-1/2}\lambda_{i,j-1/2})}, \quad (15)$$

where σ is the CFL number and the λ's are the maximum absolute values of the eigenvalues of the flux Jacobian matrix on the corresponding control volume edges.

To increase the rate of convergence of the explicit scheme we apply local time stepping, i.e., each point is advanced according to its own stability time step. In some calculations presented in this paper we apply global time stepping where a uniform time step is chosen equal to the minimum of all local time steps.

Boundary Conditions

For the flow around an airfoil there are two types of boundaries. The far field boundary due to the finite extent of the computational domain and the solid wall. In the far field we permit subsonic inflow or outflow. We use a method which takes the incoming and outgoing characteristics into account. Depending on whether the boundary is an inflow or outflow boundary we extrapolate one or three Riemann invariants from the inner field and set the remaining Riemann invariants to their value at infinity [6].

The only physical condition for inviscid flow over a solid wall is the impermeability of the solid wall which is equivalent to the normal velocity on the solid wall being equal to zero. As numerical boundary conditions we extrapolate the density, the tangential velocity, and the pressure. Due to the use of a C-grid the trailing edge becomes multi-valued. We average the values of the state vectors at the trailing edge after every stage of the Runge–Kutta scheme.

To initialize the flow field, we set all dependent variables equal to their values at infinity determined by the Mach number, M_∞, and the angle of attack, α.

3. NUMERICAL RESULTS

We calculated the well-known test case of inviscid flow around an NACA0012 airfoil at $M_\infty = 0.8$ and $\alpha = 1.25°$ [11]. With this combination of free-stream Mach number and angle of attack the flow is transonic. The solution has a strong shock on the upper surface of the airfoil, a weak shock on the lower surface, and a weak contact discontinuity in the wake. The grid we use is a C-grid with 289×65 grid points where 160 points are located on the airfoil and 65 points in the wake. The CFL number for the time step used here is CFL $= 0.6$.
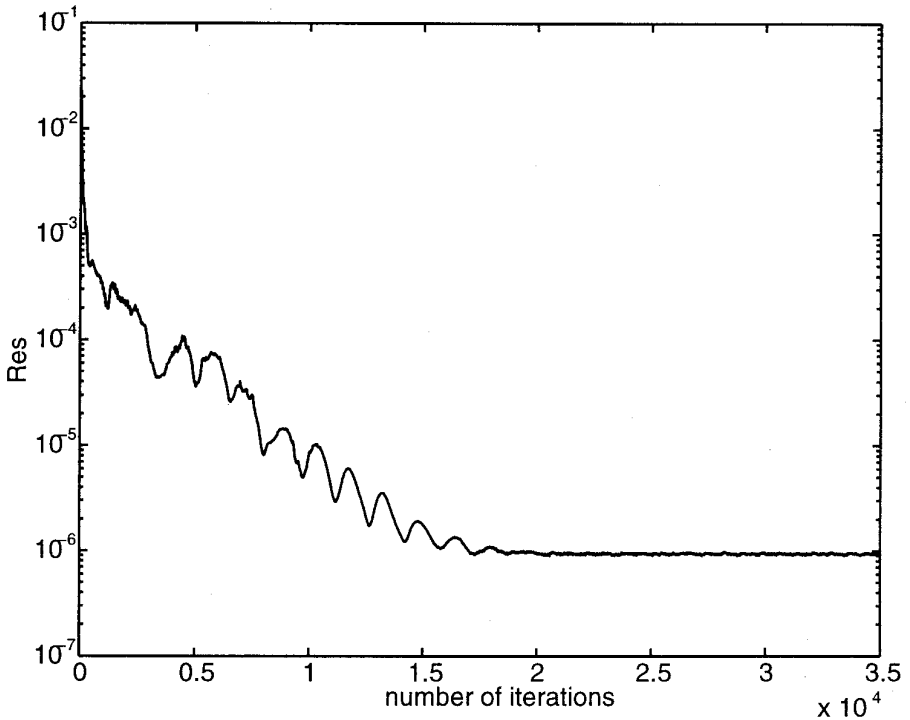
FIG. 3. Convergence history of the residual of the density with the explicit method at $M_\infty = 0.8$ and $\alpha = 1.25°$ with CFL = 0.6.

In Fig. 4 a contourplot of the pressure shows a strong shock on the upper side of the airfoil and a weak shock on the lower side of the airfoil which is in agreement with the results in [1, 3]. The strong shock on the upper side is captured with only one grid point in the shock which can be seen in Fig. 5 where the pressure coefficient c_p, defined by

$$c_p = \frac{p - p_\infty}{\frac{1}{2}\rho_\infty U_\infty^2},\tag{16}$$

is plotted. For the lift and drag we find the values $c_l = 0.348657$ and $c_d = 0.021980$.

As can be seen in Fig. 3 the solution does not converge to machine accuracy. This result is in agreement with literature (see [4]). If we change the spatial discretization from the third-order MUSCL scheme to the first-order scheme of Roe or to the second-order scheme of Jameson [12] we do get a machine accurate solution, consistent with the findings in [15]. Therefore, it appears that the lower amount of dissipation in the MUSCL scheme (8) compared with Roe's and Jameson's scheme [1], prevents the solution to converge to machine accuracy.

Another explanation for the fact that the convergence of the MUSCL scheme stalls is often explained by the non-differentiability of the limiter function (10) [3, 4]. According to [3] this phenomenon is independent of the time stepping method.
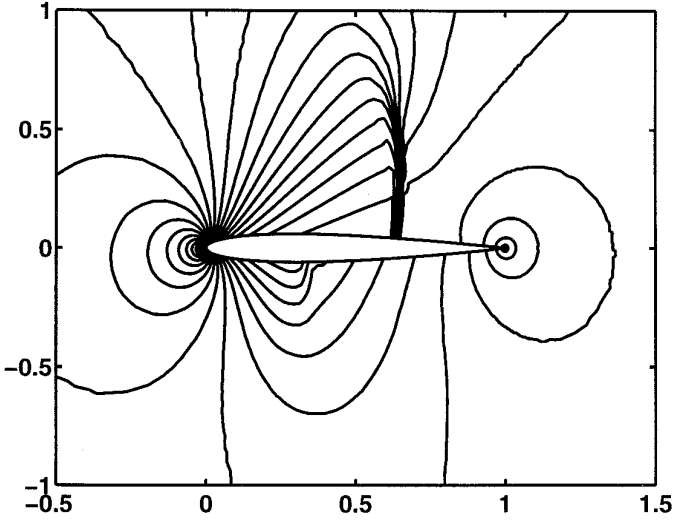
FIG. 4. Contourplot of the pressure for $M_\infty = 0.8$ and $\alpha = 1.25°$ using the MUSCL scheme.

In the next section we show that with a proper implicit scheme we can achieve a machine accurate solution with the minmod limiter.

4. IMPLICIT METHOD

In the previous section we established that it is not possible to obtain a machine accurate solution with the explicit Runge–Kutta scheme in combination with the MUSCL scheme and the minmod limiter. In this section we formulate an implicit factorization method which, as will be shown in Section 5, enables a decrease of the residual to machine accuracy.

The discrete version of (1) for the Euler backward scheme can be written as

$$q_{i,j}^{n+1} = q_{i,j}^n - \Delta t F_{i,j}(q^{n+1}), \tag{17}$$

where the superscript n labels the time level and $F_{i,j}$ is the total numerical flux in the grid point (i, j). The Euler backward scheme is first-order accurate in time, but this is not a concern here since we are only interested in the steady-state solution. First-order Taylor expansion of F around q^n yields

$$\left(\frac{I}{\Delta t} + \frac{\partial F}{\partial q}(q^n) \right) \Delta q_{i,j} = -F_{i,j}(q^n), \tag{18}$$

where $\partial F/\partial q$ is the symbolic representation of the Jacobian matrix of F and $\Delta q_{i,j} = q_{i,j}^{n+1} - q_{i,j}^n$. For infinite Δt and exact Jacobian matrix this scheme is equal to Newton iteration for $F(q) = 0$, However, it is not possible to obtain the exact Jacobian matrix at a reasonable cost. Therefore, we approximate the Jacobian as in [13]. Due to the five point stencil of Roe's scheme in 2D we get a Jacobian
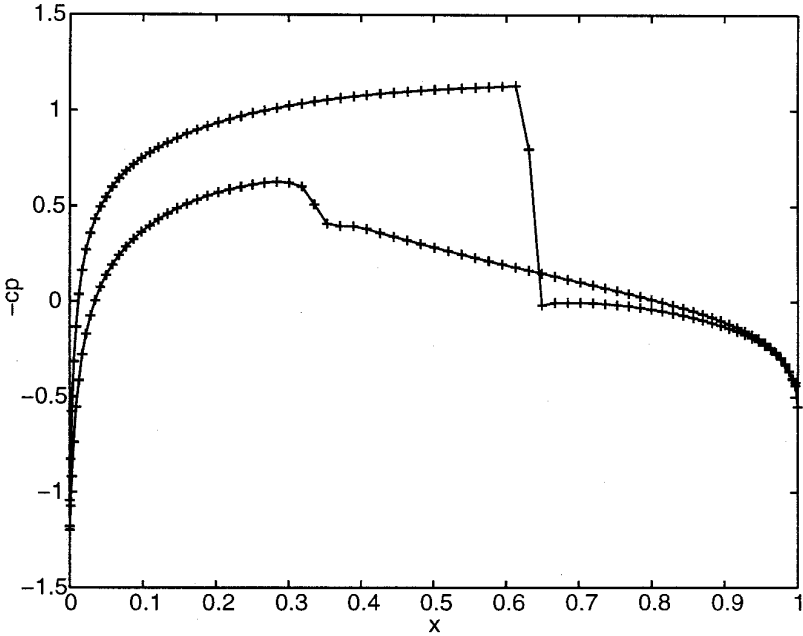
FIG. 5. The pressure coefficient c_p along the surface of the airfoil for $M_\infty = 0.8$ and $\alpha = 1.25°$ using the MUSCL scheme.

matrix with five bands of 4×4-matrices. The five blocks for a grid point (i, j) are given by

$$
\begin{aligned}
D_{i,j} &= A_{i-1/2,j}^+ - A_{i+1/2,j}^- + A_{i,j-1/2}^+ - A_{i,j+1/2}^- \\
N_{i,j} &= A_{i,j+1/2}^- \\
S_{i,j} &= -A_{i,j-1/2}^+ \\
E_{i,j} &= A_{i+1/2,j}^- \\
W_{i,j} &= -A_{i-1/2,j}^+,
\end{aligned}
\tag{19}
$$

where D, N, S, E, and W stand for diagonal, north, south, east, and west contribution. The matrices A^+ and A^- are determined by the positive and negative eigenvalues of the flux Jacobian matrix

$$
A = R\Lambda L = R(\Lambda^+ + \Lambda^-)L = R\Lambda^+ L + R\Lambda^- L = A^+ + A^-.
\tag{20}
$$

The delta formulation in (18) allows the use of an approximation of the Jacobian matrix without changing the steady-state solution. If the iteration process converges it follows from (18) that the flux equals zero in all grid points and hence the solution satisfies the stationary discrete equations. The matrix on the left-hand side in (18) can be rewritten

$$\frac{I}{\Delta t} + \frac{\partial F}{\partial q} = \left(\frac{I}{\Delta t} + D + N + S + E + W\right)$$

$$= \left(\frac{I}{\Delta t} + D + N + E\right)\left(\frac{I}{\Delta t} + D\right)^{-1}\left(\frac{I}{\Delta t} + D + S + W\right)$$

$$-(N + E)\left(\frac{I}{\Delta t} + D\right)^{-1}(S + W), \tag{21}$$

in which D, N, S, E, and W are the contribution to $\partial F/\partial q$ from the corresponding parts in (19). Neglecting the last term, which is $\mathcal{O}((\Delta t)^2)$ compared to the first term, we obtain the following implicit factorization scheme, which is similar to the scheme used in [20], however, with a different approximation of the Jacobian:

$$\left(\frac{I}{\Delta t_{i,j}} + D + N + E\right)\left(\frac{I}{\Delta t_{i,j}} + D\right)^{-1}\left(\frac{I}{\Delta t_{i,j}} + D + S + W\right)\Delta q_{i,j} = -F(q_{i,j}^n). \tag{22}$$

This system consists of a lower, upper, and diagonal matrix and can be solved in two steps:

$$\left(\frac{I}{\Delta t_{i,j}} + D + N + E\right)\Delta q_{i,j}^* = -F(q_{i,j}^n)$$

$$\left(\frac{I}{\Delta t_{i,j}} + D + S + W\right)\Delta q_{i,j} = \left(\frac{I}{\Delta t_{i,j}} + D\right)\Delta q_{i,j}^* \tag{23}$$

$$= -F(q_{i,j}^n) - N\,\Delta q_{i,j+1}^* - E\,\Delta q_{i+1,j}^*.$$

The last line in (23) shows that this factorization method can be regarded as two sweeps of the point Gauss–Seidel method where the direction in which the variables are solved changes in the second sweep but no intermediate update of the flux or the numerical Jacobian matrix is computed. Because of the topology of the C-grid the grid is cut into two parts separated by the wake centerline and the stagnation line to retain symmetry for zero angle of attack and a symmetric grid.

The boundary condition at the solid wall is treated explicitly in the same way as for the explicit scheme. The far field boundary condition is treated implicitly.

5. NUMERICAL RESULTS FOR THE IMPLICIT SCHEME

In this section we show results for the same test case as in Section 3 obtained with the implicit method defined in the previous section. A study of the difference of the residual for the explicit method and the implicit method is presented.

The time step for the implicit scheme is determined in the same way as the stability time step for the explicit scheme. Local time stepping is used to accelerate convergence. Since the Euler Backward scheme is A-stable we increase the CFL number as much as possible. In theory it should be possible to choose the CFL number infinite. We find that it is possible to increase the CFL number considerably
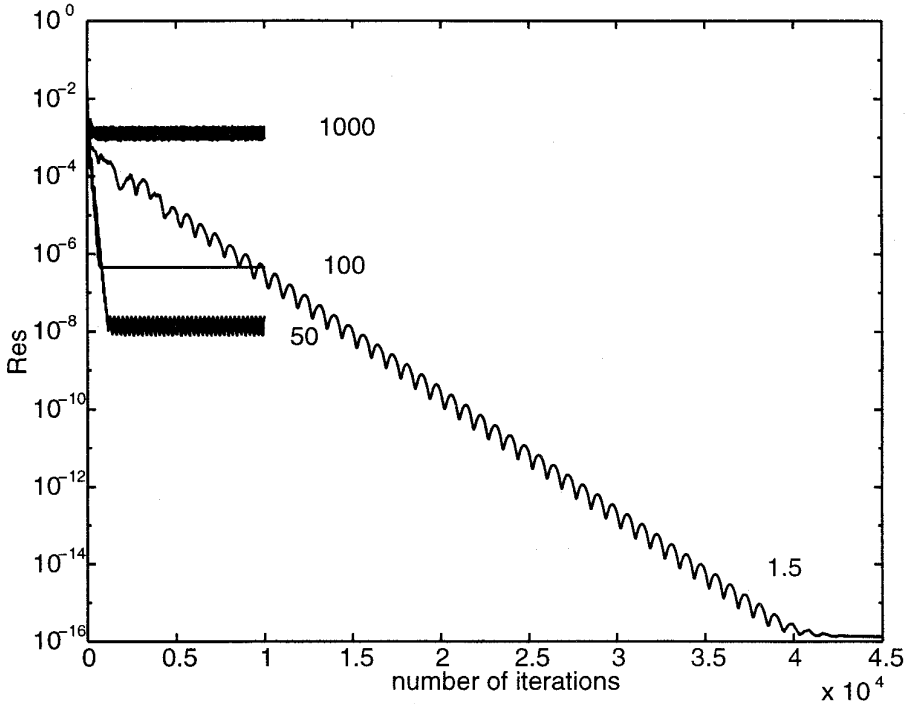
FIG. 6. Convergence history of the residual of the density with the factorization method and several CFL numbers for $M_\infty = 0.8$ and $\alpha = 1.25°$.

compared with the CFL number for the explicit scheme. A threshold value of the CFL number of about 1000 is encountered, above which no convergence takes place. The occurrence of a threshold in the CFL number can be due to the truncation error in (22) which has a more pronounced effect if the time step increases. Another reason may be that we do not treat the solid wall implicitly or the fact that the stability analysis is based on a linearized equation.

As can be seen in Fig. 6 the final residual level of the factorization method depends on the CFL number. For large CFL numbers the convergence is fast but a stall occurs. If we decrease the CFL number the convergence rate and the final residual level decrease. Although a different method was used this effect has also been observed in [10]. For the choice CFL = 1.5 we obtain a machine accurate solution with the minmod limiter. Fast convergence to machine accuracy can be obtained if we start with CFL = 50 and switch to CFL = 1.5 when the solution reaches the minimum residual level for CFL = 50. In Fig. 7 it is shown that after the switch to the lower CFL number a sharp drop of the residual occurs after which the evolution of the residual becomes similar to a run with fixed CFL = 1.5. The number of iterations needed for machine accuracy is decreased by a factor 2 compared to the run with CFL = 1.5.

In (22) we use the NE-SW combination of the factorization. In a method where the NE-SW factorization and the NW-SE version are applied alternatingly the convergence rate increases for large CFL number but the final residual level remains
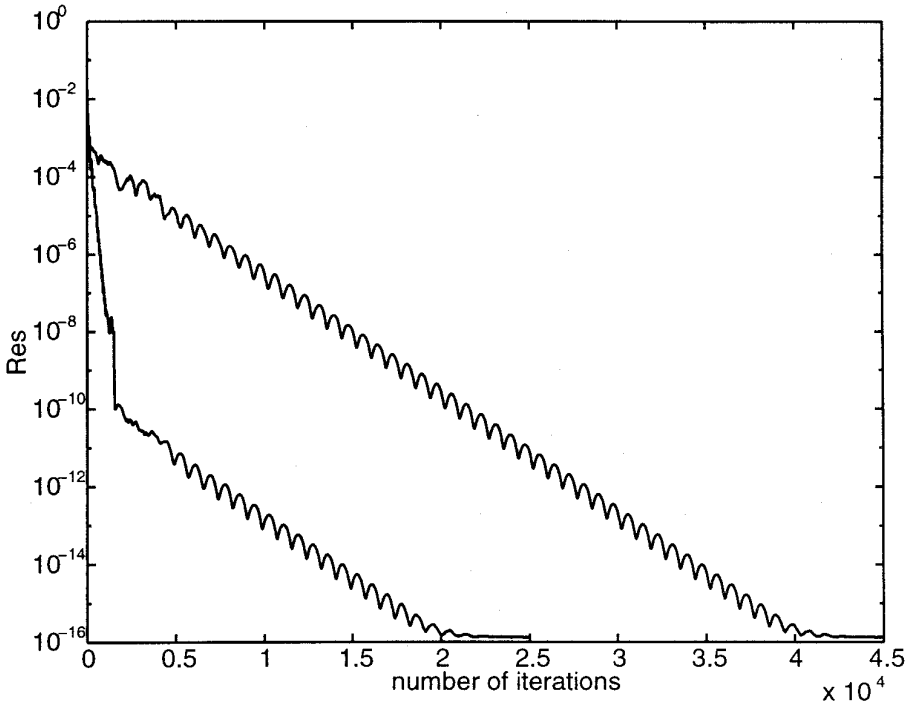
FIG. 7. Convergence history of the residual of the density with the factorization method for $\alpha = 1.25°$ and $M_\infty = 0.8$. The upper line is calculated with CFL $= 1.5$ and the lower with a combination of CFL $= 50$ and CFL $= 1.5$.

the same. The threshold value for the CFL number does not change either. For the choice of CFL $= 1.5$ no convergence acceleration occurs over the pure NE-SW method. Another version of the factorization method is the NS-EW combination which is equivalent to the DD-ADI method described in [7]. However, we do not obtain a machine accurate solution with this method.

When comparing the solution obtained with the explicit method and the factorization method (22) with CFL $= 1.5$ there is no difference in the lift and drag up to at least six digits. The question that arises is what causes the difference in the final residual level between the two methods? Is it due to a physical instability or is it a numerical phenomenon? To study the difference between the solutions we proceed from the machine accurate solution obtained with the factorization method. We use this solution as initial state and continue with the explicit method using global time stepping and CFL $= 0.6$. Figure 8 shows that the residual after the restart has an exponential growth until it reaches a level which is slightly lower than the final value of the residual in Fig. 3 which is obtained with local time stepping.

In Fig. 9 the evolution of the density in a specific grid point in the wake region is plotted. Initially the solution appears almost constant in time but as the dominant instability has sufficiently grown the solutions starts oscillating with an exponential increase of amplitude until the amplitude saturates. The
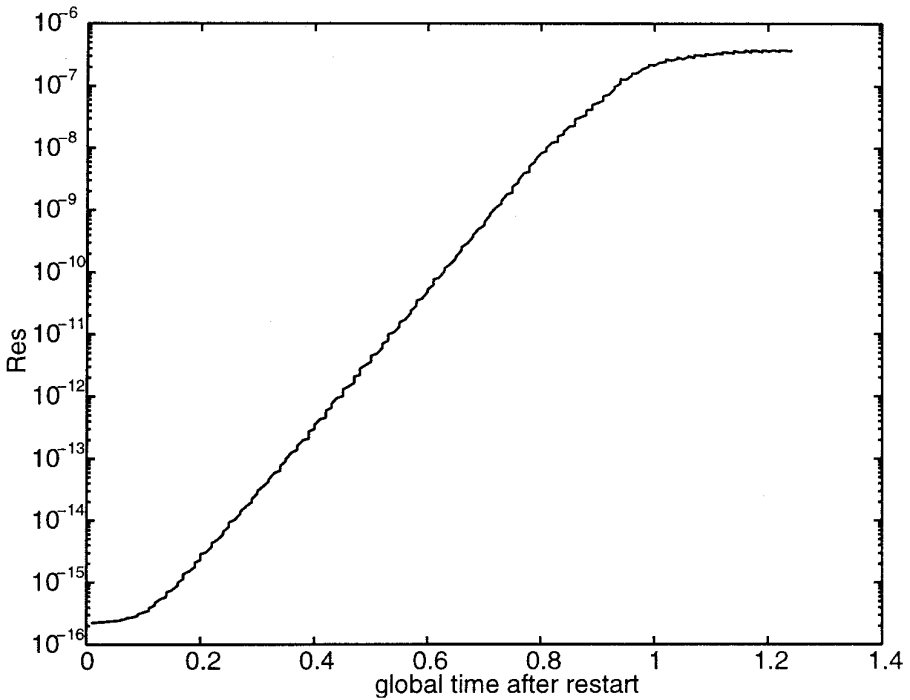
FIG. 8.   Residual as a function of time after a restart with the explicit scheme with CFL = 0.6, $\alpha = 1.25°$, $M_\infty = 0.8$, and global time stepping.

oscillation appears to contain several different frequency modes. The effects shown in Fig. 8 and Fig. 9 are very similar to shear layer instabilities as studied in [8] and results found from computations of a flow along a flat plate and mixing layers as described in [9]. This may indicate that we are dealing with a physical phenomenon. The region where the amplitude of the oscillations is significantly different from zero is bounded and located just behind the trailing edge where a contact discontinuity exists due to a difference in tangential velocity above and below the airfoil.

To exclude the effect of this discontinuity we have performed similar calculations for $\alpha = 0°$ and $M_\infty = 0.8$. The final value of the residual for the explicit method is three decades lower than for $\alpha = 1.25°$ but again a stall in the convergence arises. With the factorization method, however, a machine accurate solution is obtained. A restart from the machine accurate solution with the explicit method and global time stepping shows no increase of the residual. Adding a random disturbance to the machine accurate solution of the order 10^{-12} and restarting with the explicit scheme using global time stepping, however, we find an increase in the residual approaching the same level as with uniform flow as initial condition.

We have calculated the steady-state solution at $\alpha = 1.25°$ with the implicit scheme for various values of ω between 1 and 2.5 using a CFL number of 1.5. For $\omega = 1$ we obtain a residual of the order 10^{-6}, for $\omega = 2.5$ we obtain a residual of the order 10^{-9}, and for $\omega = 1.25$, $\omega = 1.5$, and $\omega = 2.0$ a machine accurate solution is obtained.
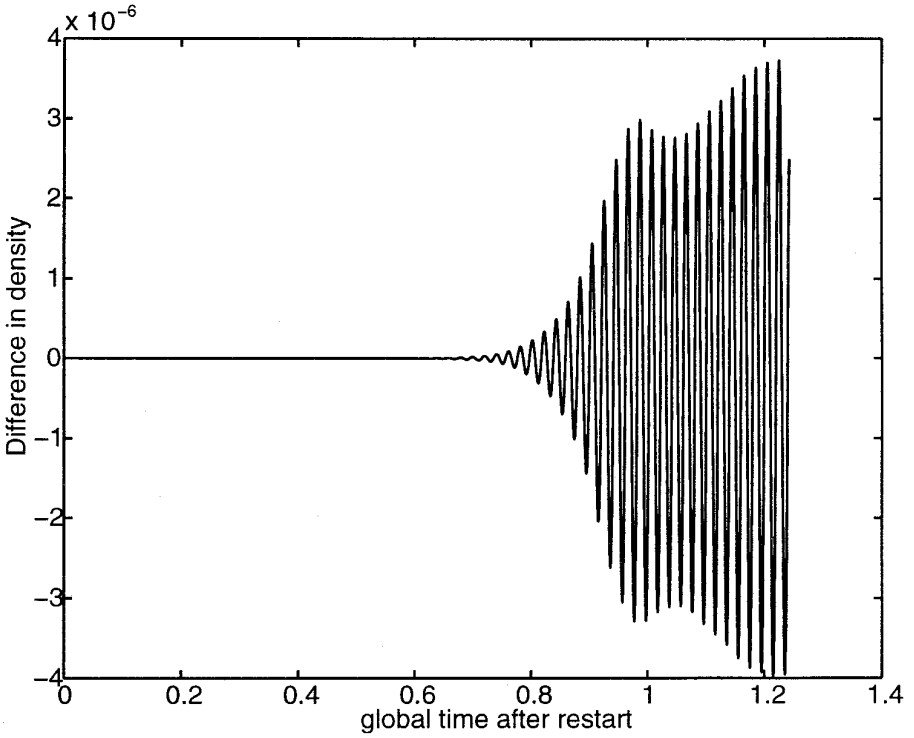
FIG. 9. Density in a grid point in the wake after restart with the explicit scheme with CFL $= 0.6$, $\alpha = 1.25°$, $M_\infty = 0.8$, and global time stepping.

The case $\omega = 1$ corresponds to the original minmod limiter where the discontinuity of the limiter is situated in the special point $(1, 1)$. The maximum value of the limiter (13) for $\omega = 2.5$ is equal to two, which is equal to the maximum value of the superbee limiter of Roe. It is known that the superbee adds a minimum amount of dissipation compared to the other symmetrical limiters making it less robust, which may explain why we do not obtain a machine accurate solution for this choice of ω. For all other choices of ω the non-differentiability is removed from a neighbourhood of $R = 1$ which seems to be a sufficient condition to obtain a machine accurate solution with the implicit scheme.

Additional calculations for $\alpha = 1.25°$ and the Van Leer limiter are performed to see whether the instability depends on the spatial discretization. The Van Leer limiter is defined as

$$\text{Lim}(a, b) = \begin{cases} \dfrac{|ab| + ab}{a + b} & \text{if } a + b \neq 0 \\ 0 & \text{if } a + b = 0. \end{cases} \tag{24}$$

To obtain the original Van Leer limiter the parameter ω is set to one in (8). For a CFL number of 1.5 we obtain a machine accurate solution with the implicit scheme. If we use this solution as initial data for the explicit scheme the residual

increases with the same growth rate as when the minmod limiter is used with $\omega = \frac{3}{2}$ (see Fig. 8).

Finally, the implicit time integration is changed to the second-order Crank–Nicolson scheme, defined by

$$q_{i,j}^{n+1} - q_{i,j}^{n} = \frac{\Delta t}{2}\left(F_{i,j}(q^{n+1}) + F_{i,j}(q^{n})\right) \tag{25}$$

for which the leading term in the truncation error is dispersive as is the case for the Runge–Kutta scheme. The factorization scheme is used here as well to solve the linear systems as in (21). The convergence behavior is similar to the convergence behavior of the Euler Backward scheme with CFL = 1.5 (Fig. 6), but the convergence stalls at the same level as the explicit scheme (Fig. 3).

Summarizing the results, we can conclude that we obtain a machine accurate solution if too much numerical dissipation is added through the spatial discretization or time integration. For the schemes with minimal numerical dissipation the convergence stalls at the final residual level of the explicit scheme.

Grid Refinement

Although there is a slight difference between $\alpha = 1.25°$ and $\alpha = 0°$, both cases show that the stationary solution found with the implicit method is unstable. This phenomenon may be caused by irregularities or coarseness of the grid. Therefore we repeat the calculation for $\alpha = 1.25°$ on a coarser and a finer grid. The coarse grid, 145×33, is obtained by deleting every other grid line in the i and j direction. The fine grid, 577×129, is obtained with a fourth order two-dimensional interpolation of the grid. For both grids we obtain a machine accurate solution with the factorization method.

Restarting with the explicit method using global time stepping we find a similar increase of the residual as on the original grid. The maximum value of the amplitude and its location are on the fine grid close to the results on the original grid. The instability phenomenon is also seen on the coarse grid. However, the region where instabilities are prominent is almost the entire region behind the airfoil which indicates that the grid is far too coarse. In Fig. 10 the residual for the three grids after a restart is plotted. It shows that the increase of the residual is maximal for the finest grid. This might be due to the fact that the dissipation on a finer grid is lower and therefore the strength of the physical instability is represented better.

Linear Stability Theory

In order to further substantiate these observations the stability of the solution obtained with the factorization method is studied in the framework of linear stability theory (LST) [19]. To this end the solution along a vertical line through the wake is inferred from the available solution on the non-orthogonal grid using fifth order accurate interpolation. Consistent with LST the parallel flow assumption is invoked and a perturbation q' of the form
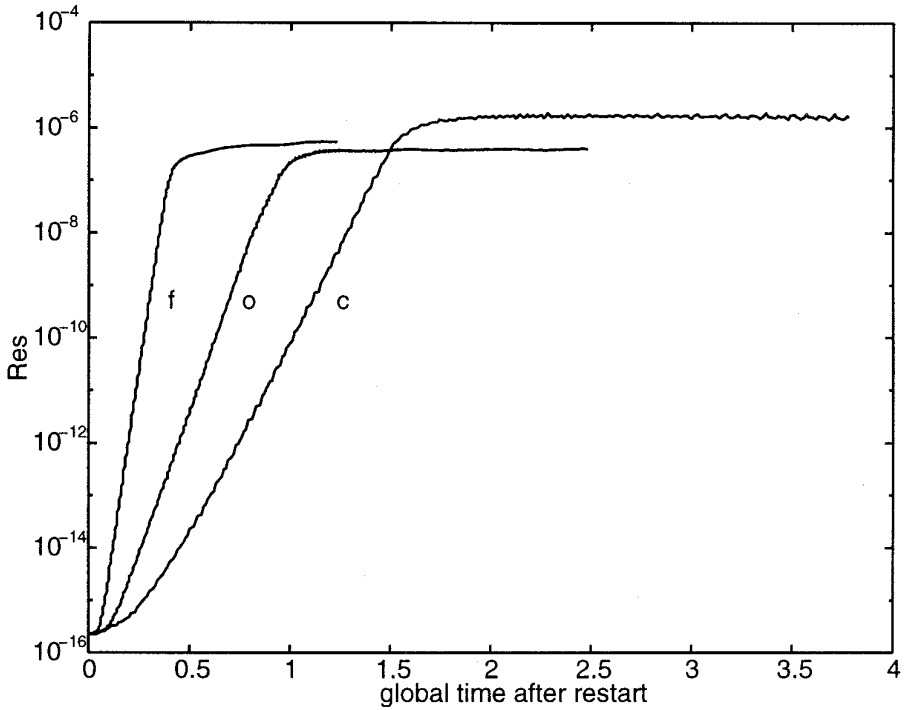
FIG. 10. Residual as a function of time after a restart with the explicit scheme with CFL = 0.6, $\alpha = 1.25°$, $M_\infty = 0.8$, and global time stepping for the three different grids where o is the original grid, f the fine grid, and c the coarse grid.

$$q' = \text{Real}[\hat{\phi}(y)\exp[i(\beta x - \omega t)]], \tag{26}$$

is determined where $\hat{\phi} = [\hat{\rho}, \widehat{\rho u}, \widehat{\rho v}, \hat{T}]$. Here we introduce the wave number β, the frequency ω, and the perturbation eigenfunction $\hat{\phi}(y)$ which are related to each other through a generalized eigenvalue problem with parameter β and eigenvalue ω. In general both β and ω can be complex. In the literature it is common practice to distinguish between temporal instability in which β is real and $\omega = \omega_r + i\omega_i$ is complex and a spatial instability with $\beta = \beta_r + i\beta_i$ and real frequency ω. Here the spatial setting is most appropriate and a small perturbation with frequency ω is predicted to grow exponentially with x, if $\beta_i(\omega) < 0$. Since there is no a priori known natural frequency ω for the instabilities in the wake we determine $\beta_i(\omega)$ for a wide range of frequencies at several x locations for the angles of attack $\alpha = 1.25°$ and $\alpha = 0°$. We observe that LST predicts both the $\alpha = 1.25°$ and $\alpha = 0°$ solutions to be unstable for a wide range of frequencies, in the region behind the airfoil, extending several chord lengths.

In Fig. 11, the dependence of β_i on ω for a typical line through the wake is plotted for the cases $\alpha = 0.0°$ and $\alpha = 1.25°$. The spatial growth rate, β_i, is about 8 times larger in the $\alpha = 1.25°$ case, which is consistent with the strongly increased residual level which arises from a restart with the explicit Runge–Kutta scheme compared to the much lower level found if $\alpha = 0°$.
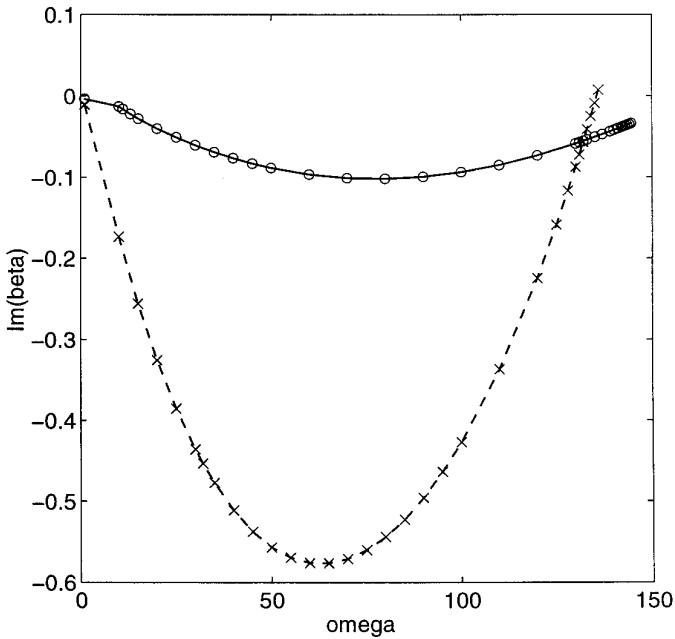
FIG. 11. β_i as a function of ω for a typical point in the wake for the cases $\alpha = 0.0°$ (solid) and $\alpha = 1.25°$ (dashed).

6. CONCLUSIONS

In this paper we have shown that it is possible to obtain a machine accurate steady-state solution to the Euler equation with the minmod limiter and an implicit time stepping scheme. We have applied an asymmetric version of the minmod limiter which removes the non-differentiability in a region where the quotient of the gradients of the solution of adjacent cells is near one. We argue that the stall of convergence of, e.g., a time explicit method is caused by a physical instability rather than by the minmod limiter.

The final values of the residual obtained with the factorization scheme depend on the CFL number. A threshold of CFL = 1000 is encountered above which the solution does not converge. Fast convergence to machine accuracy can be obtained by starting with a high CFL number and then decreasing the CFL number.

Comparison of the solution obtained with the explicit scheme and the implicit scheme for two different angles of attack, $\alpha = 1.25°$ and $\alpha = 0°$, shows that the machine accurate solution of the implicit scheme is unstable. If we change the limiter to Van Leer's limiter (24), thus changing the spatial discretization, we observe the same instabilities. Calculations performed with the second-order implicit Crank–Nicolson time integration show a stall in convergence similar to the Runge–Kutta scheme which indicates that a machine accurate solution can only be obtained if too much numerical dissipation is added through either the spatial discretization or time integration. For all schemes with a minimal amount of numerical dissipation the convergence stalls. A grid refinement study shows that the region of instability

does not vanish on a very fine grid. We have shown that this instability is also predicted by linear stability theory for both angles of attack.

Although there is an instability in the mean flow, it is very weak and relevant quantities such as the drag and lift are not affected within engineering accuracy. The lift and drag for the explicit method and for the implicit method, with CFL number up to 100, are the same up to at least six digits. Still, the results show that a stall of convergence is not always due to the numerical scheme but may be caused by a small scale physical phenomenon that cannot be observed if the numerical scheme is too dissipative.

Finally, large scale applications, e.g., three-dimensional viscous computations, with the factorization method require high memory usage and large computation time. Therefore the performance on parallel platforms is of major importance. Preliminary results with parallelization are promising and are a topic of current research.

ACKNOWLEDGMENT

REFERENCES

1. J. W. van der Burg, *Numerical Methods for Transonic Flow Calculations*, Ph.d. thesis (University of Twente, The Netherlands, 1992).

2. B. Van Leer, Towards the ultimate conservative difference scheme. II. Monotomicity and conservation combined in a second-order scheme, *J. Comput. Phys.* **14,** 361 (1974).

3. V. Venkatakrishnan, Convergence to steady state solutions of the Euler equations on unstructured grids with limiters, *J. Comput. Phys.* **118,** 120 (1995).

4. V. Venkatakrishnan, Preconditioned conjugate gradient methods for the compressible Navier–Stokes equations, *AIAA J.* **29,** 1092 (1991).

5. R. Leveque, *Numerical Methods for Conservation Laws*, Lectures in Mathematics (ETH Zürich, Birkhäuser Verlag, 1992).

6. P. L. Roe, Characteristic-based schemes for the Euler equations, *Ann. Rev. Fluid Mech.* **18,** 337 (1986).

7. J. Bardina and C. K. Lombard, Three dimensional hypersonic flow simulations with the CSCM implicit upwind Navier–Stokes method, AIAA 8th CFD Conference, AIAA Paper 87-1114-CP, 1987.

8. W. Blumen, Shear layer instability of an inviscid compressible fluid, *J. Fluid. Mech.* **40,** 769 (1970).

9. B. Geurts, B. Vreman, and H. Kuerten, Comparison of DNS and LES of transitional and turbulent compressible flow: flat plate and mixing layer, in *Application of Direct and Large Eddy Simulation to Transition and Turbulence, AGARD Conference, Proceedings 551, 5.1–14, 1994.*

10. E. Issman, G. Degrez, and H. Deconinck, Implicit upwind residual-distribution Euler and Navier–Stokes solver on unstructured meshes, *AIAA J.* **34,** No. 10 (1996).

11. H. Yoshihara and P. Sacher, *Test Cases for Inviscid Flow Field Methods*, AGARD-AR-211, 1985.

12. A. Jameson, *Transonic Flow Calculations*, MAE-rapport 1651 (Princeton University, 1983).

13. H. C. Yee, Construction of explicit and implicit shock capturing methods, *J. Comput. Phys.* **68,** 151 (1987).

14. H. C. Yee, *Computational Fluid Dynamics*, von Karman Institute for Fluid Dynamics, Lecture Series 1989-04, 1989.

15. L. E. Eriksson and A. Rizzi, Computer-aided analysis of the convergence to steady state of discrete approximations to the Euler equations, *J. Comput. Phys.* **57,** 90 (1985).

16. T. S. Park and J. H. Kwon, An improved multistage time stepping for second order upwind TVD schemes, *Comput. Fluids* **25,** No. 7, 629 (1996).

17. A. Harten and S. Osher, Uniformly high-order accurate non-oscillatory schemes I, *SIAM J. Numer. Anal.* **24,** No. 2, 279 (1987).

18. P. K. Sweby, High resolution schemes using flux limiters for hyperbolic conservation laws, *SIAM J. Numer. Anal.* **21,** No. 5, 995 (1984).

19. L. M. Mack, *Boundary Layer Stability Theory*, Special Course on Stability and Transition of Laminar Flow, AGARD CP-551, 1984.

20. S. Yoon and A. Jameson, Lower-upper symmetric-Gauss–Seidel method for the Euler and Navier–Stokes equations, *AIAA J.* **26,** No. 9 (1988).